RSC Advances

ROYAL SOCIETY OF CHEMISTRY

www.rsc.org/advances

RSC Advances

ARTICLE

Polyvinylpyrrolidone-stabilized magnetic nickel nanochains for cancer hyperthermia and catalysis applications

Jian Wu,[a,b] Wei Zhou,[c] Qingmei Cheng,[d] and Jinglei Yang[*a]

In this study, we report a novel polyvinylpyrrolidone-stabilized magnetic nickel nanochains (Ni-NC@PVP) using a simple solvothermal method for potential cancer hyperthermia and catalytic applications. The water-soluble Ni-NC@PVP exhibits excellent magnetic hyperthermia properties and low toxicity. In order to investigate the apoptotic hyperthermia efficacy of Ni-NC@PVP in skin cancer cell, we also explore the interaction of Ni-NC@PVP with cancer cells, which exhibits excellent antitumor efficacy on B16 cells. In addition, as a magnetically separable catalyst, it also shows excellent catalytic activity and durability for the selective hydrogenation of acetophenone to 1-phenylethanol. The enhanced performance demonstrates the possibility for designing new multifunctional nanomaterial with improved performances for biomedical therapies and green catalysis.

1 Introduction

Magnetic nanomaterials play an important role in the biomedicine, catalysis and environmental fields and so on due to their low toxicity and magnetic properties.[1-3] Particularly, the nickel nanomaterials are very promising candidates for magnetic hyperthermia therapy and catalytic applications.[4-10] Recently, harmless magnetic thermal therapy has attracted more attention due to using an alternating magnetic field (AMF) to heat magnetic nanomaterials embedded within tissue.[11] Up to date, many kinds of magnetic nanomaterials have been shown to heat effectively using AMF and studied in vitro and in vivo for magnetic hyperthermia therapy, such as iron oxide, iron carbide, iron nanoparticles, iron-nickel microdiscs and so on.[12-20] Despite tremendous efforts, it remains highly imperative to pursue suitable magnetic nanomaterials for magnetic thermal therapy. Although Ni nanomaterials with various morphologies have been synthesized, including rods, belts, triangular plates, chains,[21-24] and other structures, little attention has been received in magnetic hyperthermia therapy.

On the one hand, the hyperthermia performance for magnetic hyperthermia therapy is not only strongly related to kinds of compounds, but also influenced by their size and morphology of nanomaterials. Recently, it is highly desirable to determine hyperthermia efficiency of iron oxide particles with mean size, in the range 15-50 nm, for internalization into mammalian cells, especially in the case of intracellular hyperthermia. Moreover, some studies reported that the nanoparticle shape influences their efficacy by enhancing their magnetic relaxivity, increasing their ability to attach to tumor cells in vitro owing to enhanced multivalent interactions between peptide-modified nanochains and cell receptors, and

amplifying their passive accumulation in vivo over spherical nanoparticle controls.[25-29] Therefore, there are indications that nanomaterials with elongated shapes and correspondingly increased surface area are more effective in vivo due to geometrically enhanced multivalent interaction between ligands and receptors.[30]

Furthermore, the nanomaterials may also cause undesirable hazardous interactions with biological systems and the environment with potential to generate toxicity.[31-33] Therefore, it is noteworthy that the toxicity of nanomaterials has to be investigated to make sure they are safe for medical applications. Moreover, the low dispersion of active metals and adequate biocompatibility are also drawbacks of metallic particles. Thus, nanomaterials are usually encapsulated or surface modified by water-soluble polymers to prevent their agglomeration and enhance their biocompatability.[34,35] In recent years, polyvinylpyrrolidone (PVP) has received special attention because of its high chemical stability, non-toxicity, and excellent solubility in many polar solvents. Metals stabilized by PVP not only exhibit a high degree of dispersibility against agglomeration. Furthermore, the modification by polymer reduces the toxicity of magnetic nanomaterials, which are suitable for application in the biomedical field. However, PVP have not been used as a support to load metal nanoparticles for magnetic hyperthermia to date.

Inspired by the aforementioned concepts, herein, we report a novel magnetic Ni nanochains (Ni-NC) functionalized by polyvinylpyrrolidone (PVP), which is synthesized using a simple one-step solvothermal approach. The Ni nanochains are consisted of the nanoparticles of diameters about 30 nm. The Ni-NC@PVP demonstrates excellent magnetic hyperthermia and low-toxicity properties. In addition, the catalyst also shows high catalytic activity and superb recycling stability for the transfer hydrogenation of

ketones.[36] Due to these advantages, the Ni-NC@PVP provides a novel promising candidate for the hyperthermia therapy and green catalysis.

2 Experimental

2.1 Reagents

The chemicals nickel(II) acetylacetonate (Ni(acac)$_2$, 95%) was purchased from Alfa Aesar. Triethylene glycol (TREG), polyvinylpyrrolidone (PVP, M $\approx$ 40,000), ethyl acetate, acetophenone, isopropanol, dimethyl sulfoxide (DMSO) and ethanol were purchased from the Shanghai Reagent Company. All chemicals were used as received without further purification.

2.2 Synthesis of Ni-NC@PVP

In a typical procedure, a mixture of analytically pure Ni(acac)$_2$ (95%) (0.0227 g, 8.4×10^{-4} mol) and PVP (2.5 g) was added into 15 mL TREG solution. After stirring for half an hour at 135 °C in an oil bath, the transparent solution was quickly transferred into a Teflon lined stainless steel autoclave with a capacity of 22 mL. The autoclave was sealed and maintained in an oven at 240 °C for 3 h, and then naturally cooled to room temperature. A light black solution was formed, which was then diluted with 40 mL ethanol and ethyl acetate (volume ratio = 1:3), centrifuged, washed several times with ethanol to remove ions and possible remnants, collected, and vacuum dried for further characterization.

2.3 Magnetic Hyperthermia Measurements

To evaluate the magnetic heating ability, the magnetic Ni-NC@PVP nanoparticles were dispersed in distilled water under ultrasonication to create a ferrofluid with a concentration of 0.1 mg mL^{-1}. The heating behaviour of magnetic nanoparticles was studied at an alternating current (AC) magnetic field amplitude of 7.96 kA m^{-1} and frequency of 200 kHz. Thermally insulated tube containing 2 mL of the samples was placed within a water-cooled copper coil (diameter 1cm). A fluoroptic thermometer (Luxtron I652) connected to a computer was used to measure the ferrofluid temperature. C6 rat glioma cells and B16 mouse melanoma cells were seeded in a 60 mm dish at a density of 1 × 10^4 cells per well. The cells were treated with Ni-NC@PVP (0.1 mg mL^{-1}) and then incubated for 12 h at 37 °C. For hyperthermia treatment, the cells were then subjected to an alternating magnetic field for 20 min (7.96 kA m^{-1}, 200 kHz). To assess the proportion of live and dead cells, C6 rat glioma cells were stained with Trypan blue dye for 30 min. Moreover, the treated B16 mouse melanoma cells were stained with nuclear dye hoechst 33342 (5 μg mL^{-1}) and propidium iodide (PI, 10 μg mL^{-1}) after incubtion for 30 min. The cells were observed by using fluorescence microscopy (Olympus IX71, Tokyo, Japan).

2.4 In Vitro Cytotoxicity Assay (MTT Assay)

The viability and proliferation of cells in the presence of Ni-NC@PVP were evaluated by 3-[4, 5-dimethylthialzol-2-yl]-2, 5-diphenyltetrazolium bromide (MTT, Sigma) assay. The assay was performed in triplicate in the following manner. C6 cells (rat glioma cells) were seeded in 96-well plates at a density of 1×10^4 cells per well in 200 μL of media and incubated overnight at 37 °C, 5% CO$_2$. The cells were then incubated with various concentrations of Ni-NC@PVP (12.5, 25, 50, 100 of μg mL^{-1}) for 24 h. Following incubation, cells were incubated in media containing 0.1 mg mL^{-1} of MTT for 1 h. Thereafter, MTT solution was removed, and precipitated violet crystals were dissolved in 200 μL/well of DMSO. The absorbance was measured at 490 nm using a Biokinetics plate reader (Bio-TekInstruments, Inc., Winooski, VT, USA).

2.5 Catalytic Test

In the standard reaction condition, Ni nanochains (2.0 mg), acetophenone (2.4 mL, 20 mmol), isopropanol (10 mL), and NaOH (0.16 g, 4.0 mmol) were placed in a 25 mL stainless steel reactor. The reactor was tightly closed, and the mixture was stirred at 423 K for 300 min. After reaction, the catalyst was separated by applying an external permanent magnet and was reused in the next cycle. The product was quantitatively analyzed by gas chromatography using a gas chromatograph (Shimadzu GC-14C) equipped with a flame ionization detector (FID) and a chiral column (30 m × 0.32 mm, 0.25 μm film thickness). The initial temperature was maintained at 75 °C for 1 min, then raised 10 °C /min to 200 °C and held at this temperature for 20 min. Argon was used as the carrier gas at a flow rate of 1.5 mL/min. The injector temperature was 230 °C and FID temperature was 230 °C.

2.6 Characterizations

Microstructure of Ni-NC@PVP was observed using the field emission scanning electron microscopy (FESEM, FEI Sirion-200) and transmission electron microscopy (TEM, Hitachi Model H-800) with an accelerating voltage of 200 kV. To reveal the structure and elemental distribution of Ni-NC@PVP, High- resolution transmission electron microscopy (HRTEM) images and energy dispersive X-ray analysis (EDX) patterns were obtained using a JEOL-2010 transmission electron microscope at an acceleration voltage of 200 kV. The crystal structure of Ni-NC@PVP was measured using XRD patterns by using a Philips X' Pert Pro Super diffractometer with Cu Kα radiation (λ = 1.54178 Å). Magnetic properties of Ni-NC@PVP were examined using a magnetic property measurement system (MPMS) 5XL Quantum design SQUID magnetometer at room temperature.

3 Results and discussion
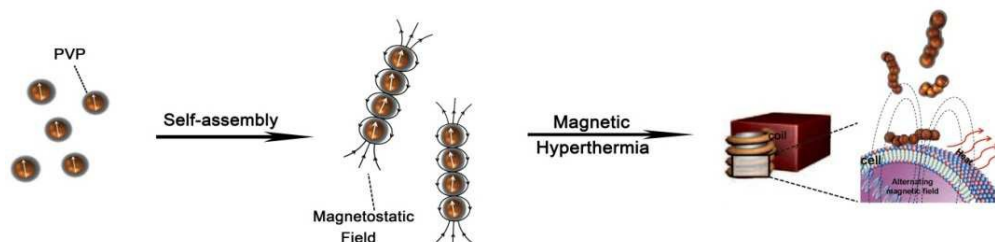
Scheme 1. Schematic illustration of the self-assembly process of Ni-NC@PVP and application for the localized magnetic hyperthermia of cancer cells

In this study, we present a novel nickel nanochains stabilized by polyvinylpyrrolidone (PVP) by the solvothermal method. The crystal phase of the nickel nanochains is examined by using X-ray diffraction technique. A typical X-ray diffraction (XRD) result of the nickel nanochains is shown in Figure 1a, which can be well indexed with lattice parameters of face-centered cubic FCC Ni (JCPDF No 04-0850). From the Scherrer formula, the average size of the nickel nanoparticles can be calculated using the FWHM of the most intense (111) peak. For nickel nanoparticles, the average crystallite size was calculated to be about 20 nm. SEM and TEM images show that the particles are mainly nanochains, each of which is composed of 30 nm Ni nanoparticles in varying numbers (Figure 1b, c and Figure S1a). The particle size evaluated from TEM micrograph ranges approximately between 20-42 nm (Figure S1b). The crystallite size calculated by XRD is ascribed to primary crystalline grain. Thus, the particle size obtained by TEM is often much larger than the XRD size. To obtain valuable insights into structural features of Ni nanochains, HRTEM images are recorded (Figure 1d). The HRTEM image shows that a typical nanoparticle is mainly of the same lattice spacings with a lattice spacing of 1.02 Å, corresponding to the interplanar distance of planes of FCC Ni, which indicates the formation of an alloy phase of nickel and shows the crystalline structure of Ni nanochains, consistent with XRD data (Figure 1a). To further reveal the structure, In Figure 1d, it is apparent that the nanoparticles are single crystals showing the planes of Ni (111) with the spacing of 0.203 nm.
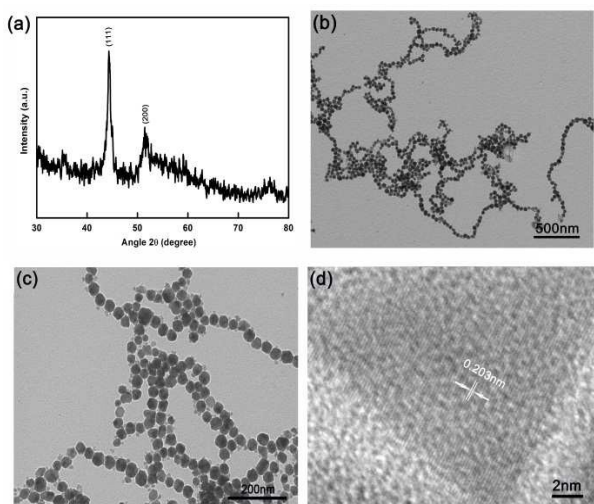

Figure 1 (a) XRD pattern of Ni-NC@PVP. (b) TEM image of nanochians structure of Ni-NC@PVP. (c) Enlarged TEM image of Ni-NC@PVP. (d) High-resolution TEM image of single Ni-NC@PVP nanoparticle structure.

We have provided more detailed characterization by FTIR and TGA in order to confirm the presence of PVP as well as quantify the amount of PVP on the nanomaterial. Figure S2a shows the characteristic peaks at 1280 and 1655 cm^{-1} attributed to the C-N linkage in which bands couple with the stretching of adjacent bands and C=O due to the interaction of the carbonyl group and Ni nanoparticle. Also, the spectrum of the coated sample consists of bands at 2940 cm^{-1}, corresponding to stretching vibrations of -CH$_2$ groups, respectively.[43-44] The PVP-coated sample has some difference compared with pure PVP, which reveals that the interaction between polymer (PVP) and metal Ni nanoparticles maybe form metal-ligand coordination bond. The result confirms that the surface of Ni nanoparticle NPs is successfully coated with PVP. Furthermore, Furthermore, TGA analysis is used to estimate

the amount of PVP on Ni-NC@PVP (Figure S2b). The thermogram is divided into two different temperature regions. The first region below 450 °C shows a weight loss and this can be ascribed to the loss of water and other solvent molecules including triethylene glycol and ethyl acetate (25-200 °C) and PVP (200-450 °C).[45-46] The second region between 450 and 800 °C shows an increase in weight of the nanomaterials due to oxidation of the Ni nanoparticles. The amount of PVP in our Ni-NC@PVP materials was estimated to be ~18 wt % by TGA.

Moreover, Ni-NC@PVP is suitable for magnetic hyperthermia and green catalysis applications due to its easy recovery from the reaction mixture by the use of an external magnetic field. Based on the above discussion, the schematic diagram of the self-assembly process is summarized and shown in Scheme 1. The single domain nanoparticles can disperse uniformly and move freely in the electrolyte solution. Upon application of a magnetic field, the nanoparticles would align and connect with each other to form short nanochains. The hydrodynamic diameter of nanoparticles is determined by DLS (Figure S3a). The main peaks for Ni-NC@PVP are centered in 40-80 nm with PDI values (0.154) and narrow size distributions as shown in Figure S3, which are larger than the TEM results. Since the nanoparticles are slightly agglomerated or assembled into nanochain, the DLS measurement is often much larger than the TEM size. Furthermore, Zeta potential measurements are carried out for Ni-NC@PVP dispersed in water. Figure S3b illustrates the zeta potential as a function of pH in the range from 2 to 10. Ni-NC@PVP's potential is positive at lower pH and becomes negative at higher pH, in agreement with previously reported.[43] From Figure S4b it can be seen that the isoelectric point is found to be about 4.5 where particles carry no net electric charge on their surfaces. The experimental results show that the Ni-NC@PVP system is more stable in high pH medium.
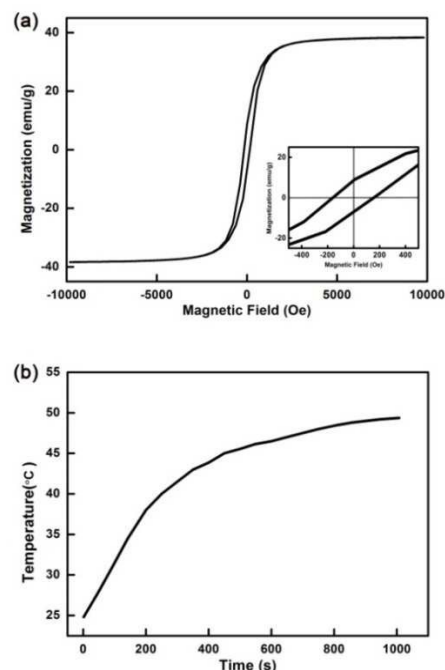

Figure 2 (a) Field-dependent magnetization curve (M-H) of Ni-NC@PVP. Inset: detail of the low field region to evaluate the coercive field. (b) Magnetic heating curve measured for Ni-NC@PVP obtained at AMF (7.96 kAm^{-1}, 200 kHz).

The magnetic properties of Ni-NC@PVP are investigated by measuring the magnetization as a function of the applied field at 300

K (Figure 2a). Ni-NC@PVP exhibits ferromagnetic behavior, as indicated by the presence of open hysteresis loops in the M-H curves. The open hysteresis loops in the low field region are shown in Figure 2a inset photograph. It is found that Ni-NC@PVP displays similar saturation magnetization (40-60 emu/g) to that of nickel nanomaterials with similar nanochain morphology and nanoparticles size about 30-50 nm.[22, 51-53] Such high saturation magnetization of Ni-NC@PVP is advantageous for magnetic guiding applications because it allows them to respond rapidly to an external magnetic field. Controlled heat generation is explored by submitting the prepared magnetic microcontainers to an alternating magnetic field (AMF). Application of Ni-NC@PVP in thermal therapy depends on the heating efficiency of Ni-NC@PVP, which is dependent on particle size, size distribution in a real sample, field frequency and amplitude of the AMF. When the Ni-NC@ PVP (0.1 mg mL^{-1}) was exposed to the AC magnetic field, the temperature increased rapidly and reached the therapeutic threshold required for cancer hyperthermia (T > 42 °C) [34] within 20 min under AMF amplitude (7.96 kA m^{-1}, 200 kHz) as shown in Figure 2b. It is found that Ni-NC@PVP displays similar magnetic heating effect to that of other magnetic nanomaterials at similar concentrations [34,47,48,50] or similar frequency [49].

To validate the applicability of Ni-NC@PVP for magnetic hyperthermia, their magnetic heating effect is evaluated under an alternating current magnetic field an AMF (7.96 kA m^{-1}, 200 kHz) as shown in Figure 3. The apoptotic hyperthermia efficacy of the Ni-NC@PVP is explored using an in vitro study. A mixture of C6 rat glioma cells (1.0×10^4 cells per well) are incubated with Ni-NC@PVP for 5 h. Then, an AMF is applied to maintain the temperature of the solution at T > 42 °C for 20 minutes using a temperature probe and an AMF transducer (Figure 3a). As a control, cells are also treated with Ni-NC@PVP alone or AMF alone, or media only (Figure 3b-d). C6 rat glioma cells are abolished by the temperature rise due to Ni-NC@PVP heating under AMF. The cells incubated with Ni-NC@PVP subjected to the magnetic field show more cell death (black arrowhead) after treatment, whereas cells that are treated with Ni-NC@PVP but without exposing to the magnetic field are unaffected (Figure 3c). As expected, control cells that are exposed to the magnetic field in the absence of Ni-NC@PVP showed no decrease in the cell viability (Figure 3d). Despite the fact that the initial cell numbers of all the experiments is leveled, the trypan blue staining procedure includes several washing steps, therefore most of the dead cells in Figure 3a are discarded and led to the cell number difference compared to the other conditions.
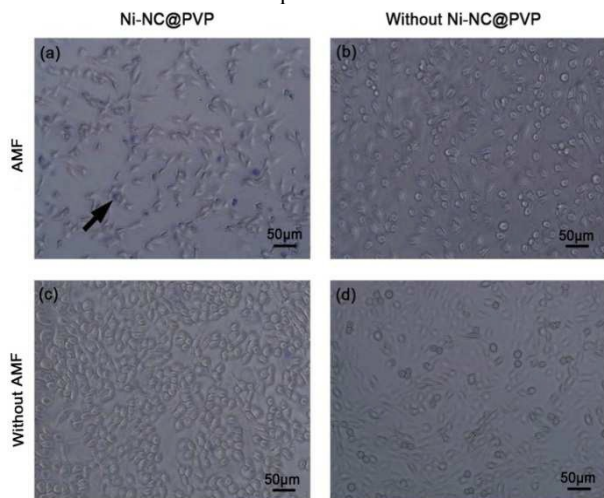

Figure 3 Micrographs show the effect of Ni-NC@PVP treatments on C6 cells with or without alternating current magnetic field,

followed by Trypan blue staining. C6 cells treated with Ni-NC@PVP (a, c) or without Ni-NC@PVP (b, d) were observed under the bright field mode of confocal microscope.
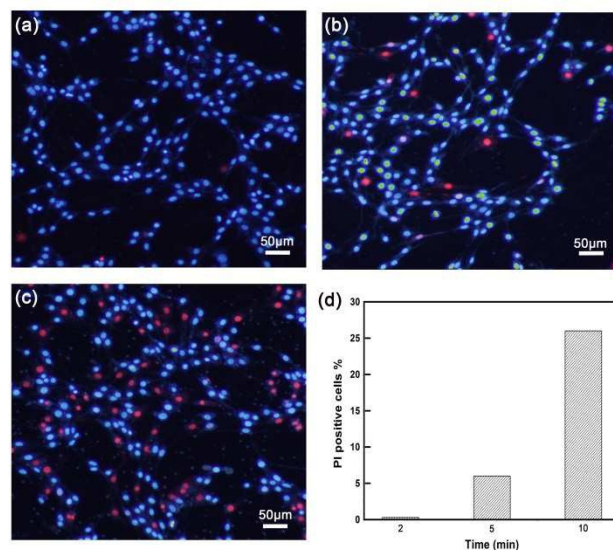

Figure 4 Fluorescence images of B16 cells treatment with Ni-NC@PVP and the subsequent application of an alternating current magnetic field. Hoechst 33342 are used to visualize the nuclei (blue) and PI to illustrate the apoptotic cells (red). (a-c) The images are obtained after treatment in 2, 5, and 10 min, respectively. (d) The percentage of dead cells treatment with Ni-NC@PVP and alternating current magnetic field after 2, 5 and 10 min (the amount of death cells is expressed as the percentage of PI-positive cells).
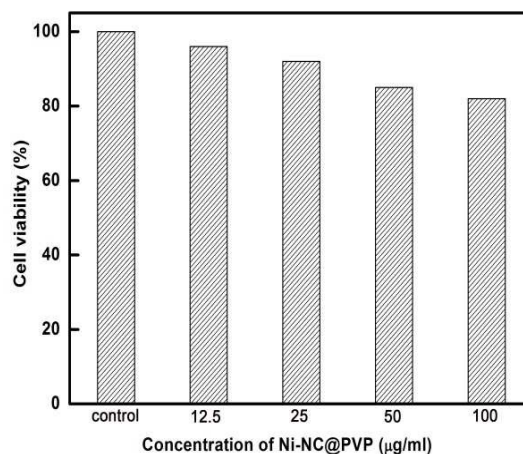

Figure 5 Cell viability of C6 cells in the presence of Ni-NC@PVP for 24 h evaluated using the MTT assay.

Furthermore, magnetic nanoparticles may be actively accumulated into the tumor tissues by guidance with an external magnetic field of suitable strength. In general, the magnetic nanoparticles in normal vessels are captured close to skin, for extracorporeally applied magnetic fields. Thus, in order to investigate the apoptotic hyperthermia efficacy of the Ni-NC@PVP in skin cancer cell, the interaction of Ni-NC@PVP is explored with B16 cells with bulk heating established. B16 cells are incubated with Ni-NC@PVP for 20 min followed by magnetic field treatment at different duration (2, 5, and 10 min). Cells grown in a medium added with Hoechst 33342 (5 μg mL^{-1}, stains the nuclei of living cells) and PI (10 μg mL^{-1},

stains the nuclei of dead cells) are calculated for each condition using Image Pro, and the results are shown in Figure 4a-c. The extent of cancer cell death is quantitatively measured from the obtained fluorescence microscopic images (Figure 4d). In the case of the Ni-NC@PVP, the cell death decreased monotonically from about 0.2% to 5% and 25% as the time of the hyperthermia treatment was increased from 2, 5, to 10 min, respectively. Our result demonstrates that Ni-NC@PVP exhibits efficient magnetic hyperthermia performance and provides a selective tool for nanomaterials induced ablation, as well as useful dosing information for future animal study. For clinical applications, a limited range of magnetic field amplitude and frequency ($H \times f < 50 \times 10^8$ Am^{-1}s^{-1}) should be used to avoid undesirable neuromuscular stimulation and nonspecific inductive heating of normal tissues.[13,34] Since the AC magnetic field used in this study had a relatively small $H \times f$ value (15.9×10^8 Am^{-1}s^{-1}), it is conceivable that the hyperthermia treatment with Ni-NC@PVP could be administered at a safe and tolerable range of magnetic field strengths without causing deleterious side effects.

The biocompatibility of nanoparticles is a key factor for their biological applications. Recently, some groups have demonstrated that the cytotoxicity of magnetic fluids depends on the concentration of nanoparticles as well as the surface coating material. To fully evaluate the possible toxic effects of Ni-NC@PVP, we evaluate the cell viability of C6 cells and B16 cells treated with different concentrations of Ni-NC@PVP for 24 h. It is shown C6 cells viability range from 97% to 82% when the concentration of Ni-NC@PVP from 12.5 to 100 μg mL^{-1}. No significant toxicity of the Ni nanochains is shown up to the concentration of 100 μg mL^{-1} on our experimental conditions (Figure 5). In the case the PVP is expected to insulate and stabilize the Ni nanoparticle, attenuating or inhibiting the possible interactions between nanochains and cell surface. In summary, Ni nanochains have an almost absent inhibitory effect on the growth and viability of cell suspension cultures compared to uncovered Ni nanomaterials.[37-41] Furthermore, the reduction of the Ni-NC@PVP toxicity is not due to a lack of cell proximity but most likely a consequence of the PVP coating.
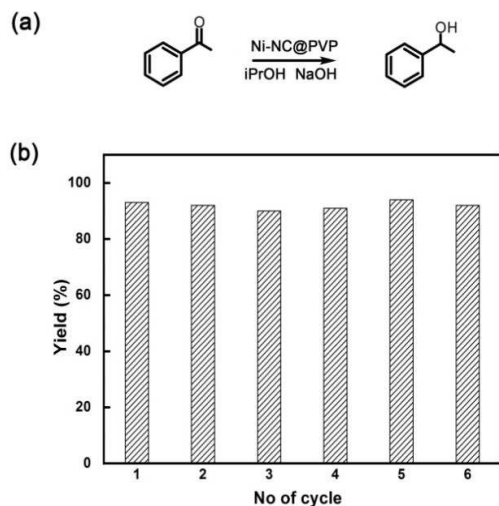

Figure 6 (a) Catalytic transfer hydrogenation of acetophenone over Ni-NC@ PVP. (b) Reusability of Ni-NC@ PVP.

Hydrogenation of acetophenone to 1-phenylethanol is of one of the most important reactions due to the significant applications of 1-phenylethanol in the pharmaceutical, fine chemicals and perfumery industries. Although some homogeneous catalysts could exclusively give a 1-phenylethanol product, the difficulties lie in product

separation and catalyst recovery.[42] Herein, the catalytic activity and reusability of the magnetic Ni-NC@PVP was investigated (Figure 6). Blank tests in the absence of the catalyst show almost negligible conversion of only 3 % and 1-phenylethanol is not found in the product. It is shown that the 1-phenylethanol products have been obtained in good to excellent yields (90-94%) as shown in Figure 6b. The acetophenone conversion is about 96-97 % (Figure S4). Figure S6 shows the kinetic profile of the reaction. After removal of catalyst, the conversion only increased 6 %, which could be attributed to the background reaction. This indicated that the reaction was catalyzed by Ni-NC@PVP catalyst. Moreover, Ni-NC@PVP can be easily harvested with magnet very well due to its good soft magnetic property (Figure 2a). After the catalytic reaction, the Ni-NC@PVP is reused after washing with absolute ethyl alcohol and treating under vacuum at 60 °C for 10 h. Our result shows that the catalyst has recycling stability for six cycles of examination without observable deterioration (Figure 6b). To evaluate the catalyst stability upon reuse, we have provided the FTIR spectra and XRD pattern of the Ni-NC@PVP before and after the catalytic studies (Figure S2 and Figure S5). The characterization result indicates the high stability of the Ni-NC@PVP. Thus, coupled with the excellent catalytic performance, the general advantages of Ni-NC@PVP, including the magnetically separable processing, stable recyclability and low cost, endow it with great catalytic property in the hydrogenation of acetophenone, as well as in some other related catalytic reactions.

4 Conclusions

In summary, we have successfully synthesized Ni nanochains coated by PVP (Ni-NC@PVP) via simple solvothermal approach for magnetic hyperthermia and catalysis properties. The surface modification approach using PVP conjugates produce highly stable and water-dispersible ferromagnetic Ni nanochains. The water-soluble Ni-NC@ PVP exhibit excellent magnetic hyperthermia properties on cancer cells with low toxicity. Moreover, magnetic nanoparticles may be actively accumulated into the tumor tissues by guidance with an external magnetic field. Thus, in order to investigate the apoptotic hyperthermia efficacy of Ni-NC@PVP in skin cancer cell, we next explore the interaction of Ni-NC@PVP with cancer cells with bulk heating established, which exhibits excellent antitumor efficacy on B16 cells. Considering these outstanding characteristics, this novel nanochians structure combined with magnetic hyperthermia may enable a safe and effective treatment of various types of cancers in the future. In addition, Ni-Ni@PVP also shows excellent catalytic activity and catalyst durability for the selective hydrogenation of acetophenone to 1-phenylethanol.

Acknowledgements

Notes and references

[a]School of Mechanical and Aerospace Engineering, Nanyang Technological University, Nanyang 639798, Singapore.

[b]State Key Laboratory of Coal Conversion, Institute of Coal Chemistry, Chinese Academy of Sciences, Taiyuan, Shanxi 030001, P. R. China.

[c] Hefei National Laboratory for Physical Sciences at the Microscale, University of Science and Technology of China, Hefei, Anhui 230026, P. R. China.

[d] Department of Chemistry, Merkert Chemistry Center, Boston College, Chestnut Hill, MA 02467. USA.

Corresponding author's email: E-mail: mjlyang@ntu.edu.sg

1   N. A. Frey, S. Peng, K. Cheng, S. Sun, *Chem. Soc. Rev.* 2009, **38**, 532.

2   G. von Maltzahn, J. H. Park, K. Y. Lin, N. Singh, C. Schwoppe, R. Mesters, W. E. Berdel, E. Ruoslahti, M. J. Sailor, S. N. Bhatia, *Nat. Mater.* 2011, **10**, 545.

3   D. Ho, X. L. Sun, S. H. Sun, *Acc. Chem. Res.* 2011, **44**, 875.

4   X. Y. Wang, R. Rinaldi, *Energ Environ. Sci.* 2012, **5**, 8244.

5   J. Dulle, S. Nemeth, E. V. Skorb, T. Irrgang, J. Senker, R. Kempe, A. Fery, D. V. ndreeva, *Ad. Funct. Mater.* 2012, **22**, 3128.

6   R. Weissleder, M. Nahrendorf, M. J. Pittet, Nat. Mater. 2014, 13, 125.

7   F. Alonso, P. Riente, M. Yus, *Acc. Chem. Res.* 2011, **44**, 379.

8   V. Polshettiwar, B. Baruwati, R. S. Varma, *Green Chem*, 2009, **11**, 127.

9   J. F. Sonnenberg, N. Coombs, P. A. Dube, R. H. Morris, *J. Am. Chem. Soc.* 2012, **134**, 5893.

10 J. C. Park, H. J. Lee, J. Y. Kim, K. H. Park, H. Song, *J. Phys. Chem. C*, 2010, **114**, 6381.

11 H. Huang, S. Delikanli, H. Zeng, D. M. Ferkey, A. Pralle, *Nat. Nanotechnol,* 2010, **5**, 602.

12 L. Lartigue, C. Innocenti, T. Kalaivani, A. Awwad, M. Sanchez Duque Mdel, Y. Guari, J. Larionova, C. Guerin, J. L. Montero, V. Barragan-Montero, P. Arosio, A. Lascialfari, D. Gatteschi, C. Sangregorio, *J. Am. Chem. Soc.* 2011, **133**, 10459.

13 L. M. Lacroix, N. F. Huls, D. Ho, X. Sun, K. Cheng, S. Sun, *Nano Lett.* 2011, **11**, 1641.

14 B. Samanta, H. Yan, N. O. Fischer, J. Shi, D. J. Jerry, V. M. Rotello, *J. Mater. Chem.* 2008, **18**, 1204.

15 S. A. Stanley, J. E. Gagner, S. Damanpour, M. Yoshida, J. S. Dordick, J. M. Friedman, *Science,* 2012, **336**, 604.

16 D. H. Kim, E. A. Rozhkova, I. V. Ulasov, S. D. Bader, T. Rajh, M. S. Lesniak, V. Novosad, *Nat. Mater,* 2010, **9**, 165.

17 A. Meffre, B. Mehdaoui, V. Kelsen, P. F. Fazzini, J. Carrey, S. Lachaize, M. Respaud , B. Chaudret, *Nano Lett.* 2012, **12**, 4724.

18 S. Brule, M. Levy, C. Wilhelm, D. Letourneur, F. Gazeau, C. Menager, C. L. Visage, *Adv.Mater.* 2011, **23**, 787.

19 P. Bilalis, A. Chatzipavlidis, L.-A. Tziveleka, N. Boukos, G. Kordas, *J. Mater. Chem.* 2012, **22**, 13451.

20 A. Villanueva, P. de la Presa, J. M. Alonso, T. Rueda, A. Martinez, P. Crespo, M. P. Morales, M. A. Gonzalez-Fernandez, J. Valdes, G. Rivero, *J. Phys. Chem. C.* 2010, **114**, 1976.

21 P. Li, R. Wang, W. Chen, C. Chen, X. Gao, A. Wee, *Nanoscale. Res. Lett.* 2009, **5**, 597.

22 W. Zhou, H. He, R. Cheng, L. Guo, C. P. Chen, J. L. Wang, *J. Phys. Chem. C.* 2009, **113**, 17355.

23 J. F. Xiong, H. Shen, J. X. Mao, X. T. Qin, P. Xiao, X. Z. Wang, Q. Wu, Z. Hu, *J. Mater. Chem.* 2012, **22**, 11927.

24 P. W. Li, W. M. Chen, W. Liu, Z. A. Li, Y. M. Cui, A. P. Huang, R. M. Wang, C. P. Chen, *J. Phys. Chem. C.* 2010, **114**, 7721.

25 E. Alphandery, C. Carvallo, N. Menguy, I. Chebbi, *J. Phys. Chem. C.* 2011, **115**, 11920.

26 J. H. Park, G. von Maltzahn, L. L. Zhang, A. M. Derfus, D. Simberg, T. J. Harris, E. Ruoslahti, S. N. Bhatia, M. J. Sailor, *Small.* 2009, **5**, 694.

27 E. Alphandery, S. Faure, O. Seksek, F. Guyot, I. Chebbi, *Acs Nano.* 2011, **5**, 6279.

28 J. H. Park, G. von Maltzahn, L. Zhang, M. P. Schwartz, E. Ruoslahti, S. N. Bhatia, M. J. Sailor, *Adv. Mater.* 2008, **20**, 1630.

29 Y. X. Hu, L. He and Y. D. Yin, *Angew. Chem. Int. Ed.* 2011, **50**, 3747.

30 J. T. Jang, H. Nah, J. H. Lee, S. H. Moon, M. G. Kim, J. Cheon, *Angew. Chem. Int. Ed.* 2009, **48**, 1234.

31 F. Zhao, Y. Zhao, Y. Liu, X. Chang, C. Chen and Y. Zhao, *Small.* 2011, **7**, 1322.

32 A. E. Nel, L. Madler, D. Velegol, T. Xia, E. M. V. Hoek, P. Somasundaran, F. Klaessig, V. Castranova, M. Thompson, *Nat. Mater.* 2009, **8**, 543.

33 T. Puzyn, B. Rasulev, A. Gajewicz, X. K. Hu, T. P. Dasari, A. Michalkova, H. M. Hwang, A. Toropov, D. Leszczynska, J. Leszczynski, *Nat. Nanotechnol.* 2011, **6**, 175.

34 K. H. Bae, M. Park, M. J. Do, N. Lee, J. H. Ryu, G. W. Kim, C. Kim, T. G. Park, T. Hyeon, *Acs Nano.* 2012, **6**, 5266.

35 L. A. Thomas, L. Dekker, M. Kallumadil, P. Southern, M. Wilson, S. P. Nair, Q. A. Pankhurst, I. P. Parkin, J. Mater. Chem. 2009, **19**, 6529.

36 K. Shimura, K.-i. Shimizu, *Green. Chem.* 2012, **14**, 2983.

37 M. Ahamed, *Toxicology in Vitro.* 2011, **25**, 930.

38 Z. Abdullaeva, E. Omurzak, C. Iwamoto, H. Ihara, H. S. Ganapathy, S. Sulaimanku-lova, M. Koinuma, T. Mashimo, *Jpn. J. Appl. Phys.* 2013, **52**, 01AJ01.

39 S. Minocha and R. J. Mumper, *Small.* 2012, **8**, 3289.

40 S. Alarifi, D. Ali, S. Alakhtani, E.S. Al Suhaibani, A. A. Al-Qahtani, *Biol. Trace. Elem. Res.* 2014, **157**, 84.

41 D. Guo, C. Wu, X. Li, H. Jiang, X. Wang, B. Chen, *J. Nanosci. Nanotechnol.* 2008, **8**, 2301.

42 P. O. Lagaditis, A. J. Lough, and R. H. Morris. *J. Am. Chem. Soc.* 2011, **133**, 9662-9665.

43 S. V. Jadhav, D. S. Nikam, V. M. Khot, N. D. Thorat, M. R. Phadatare, R. S. Ningthoujam, A. B. Salunkhe , S. H. Pawar. *New J. Chem.* 2013, **37**, 3121-3130.

44 R. Kumar , P. F. Siril. *RSC Adv.* 2014, **4**, 48101-48108.

45 V. M. Shinde, G. Madras. *RSC Adv.* 2014, **4**, 4817-4826.

46 Y. Cheng, B. Zou, C. Wang, Y. Liu, X. Fan, L. Zhu, Y. Wang, H. Ma, X. Cao. *CrystEngComm*, 2011, **13**, 2863-2870.

47 D. Yoo, H. Jeong, S. H. Noh, J. H. Lee and J. Cheon, *Angew Chem Int Edit,* 2013, **52**, 13047-13051.

48 E. Peng, J. Ding and J. M. Xue, *New J. Chem*, 2014, 38, 2312-2319.

49 P. Bilalis, A. Chatzipavlidis, L. A. Tziveleka, N. Boukos and G. Kordas, *J Mater Chem*, 2012, **22**, 13451-13454.

50 X. L. Liu, E. S. G. Choo, A. S. Ahmed, L. Y. Zhao, Y. Yang, R. V. Ramanujan, J. M. Xue, D. Di Fan, H. M. Fan and J. Ding, *J Mater Chem B,* 2014, **2**, 120-128

51   P. W. Li, W. M. Chen, W. Liu, Z. A. Li, Y. M. Cui, A. P. Huang, R. M. Wang and C. P. Chen, *J Phys Chem C*, 2010, **114**, 7721-7726.

52   N. Wang, X. Cao, D. S. Kong, W. M. Chen, L. Guo and C. P. Chen, *J Phys Chem C*, 2008, **112**, 6613-6619.

53   L. He, W. Z. Zheng, W. Zhou, H. L. Du, C. P. Chen and L. Guo, *J Phys-Condens Mat*, 2007, **19**. 036216.

Supporting Information

Polyvinylpyrrolidone-stabilized magnetic nickel nanochains for cancer hyperthermia and catalysis applications

Jian Wu,[a,b] Wei Zhou,[c] Qingmei Cheng,[d] and Jinglei Yang[*a]

a School of Mechanical and Aerospace Engineering, Nanyang Technological University, Nanyang 639798, Singapore.
b State Key Laboratory of Coal Conversion, Institute of Coal Chemistry, Chinese Academy of Sciences, Taiyuan, Shanxi 030001, P. R. China.
c Hefei National Laboratory for Physical Sciences at the Microscale, University of Science and Technology of China, Hefei, Anhui 230026, P. R. China.
d Department of Chemistry, Merkert Chemistry Center, Boston College, Chestnut Hill, MA 02467. USA.
Corresponding author's email: E-mail: mjlyang@ntu.edu.sg

S1 Characterizations

Attenuated total reflectance-Fourier transform infrared spectroscopy (ATR-FTIR) spectra were recorded by Perkin Elmer Frontier FT-NIR/MIR spectrometers. Spectra were obtained with resolution of 2 cm^{-1} and 16 scans. Thermal gravimetric analysis (TGA) of the as-synthesized samples were carried out on a Shimadzu TA-50 thermal analyzer at a heating rate of 10 °C/min from room temperature to 800 °C in air. Zeta potential and DLS measurements were performed using a Malvern 4800 Autosizer employing a 7132 digital correlator for the determination of the hydrodynamic diameter. Measurements were taken in water. HCL (0.2 M) and NaOH (0.2 M) are used to tune the pH from 2 to 10. The pH adjustment is achieved by using pH meters. The reported zeta potential values were an average of three measurements.
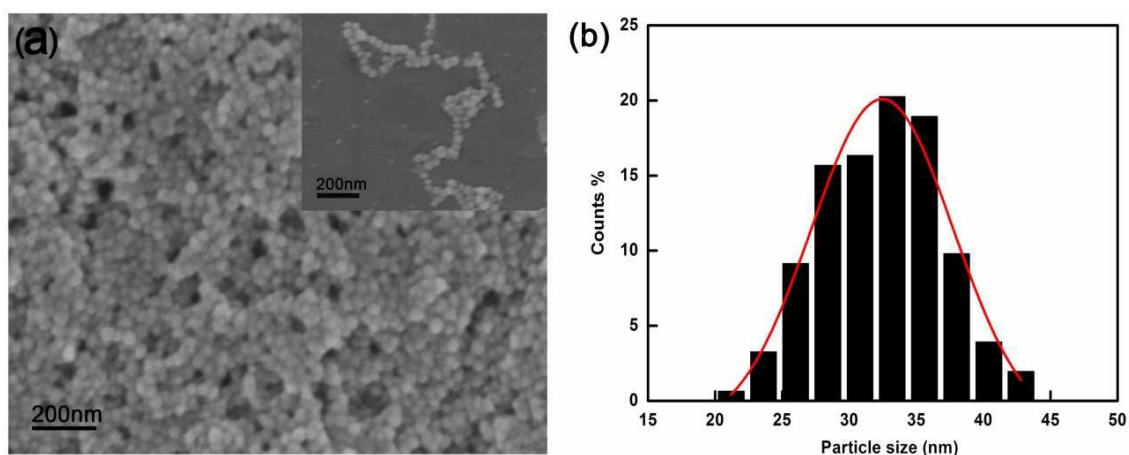

Figure S1 (a) SEM images of Ni-NC@PVP. (b) The histogram of grain size distribution of Ni-NC@PVP from TEM in Figure 1c.
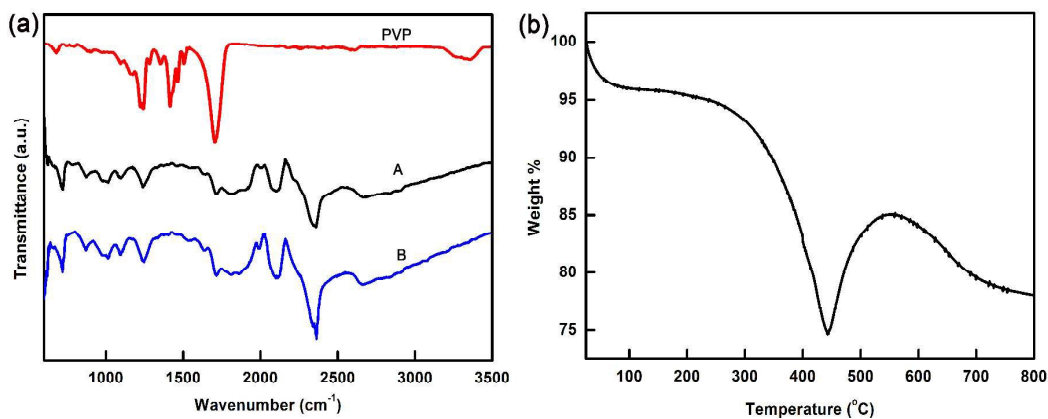
Figure S2 (a) FTIR spectra of Ni-NC@PVP before (A) and after (B) the catalytic test reaction and pure PVP. (b) Thermogravimetric analysis (TGA) under air of Ni-NC@PVP.
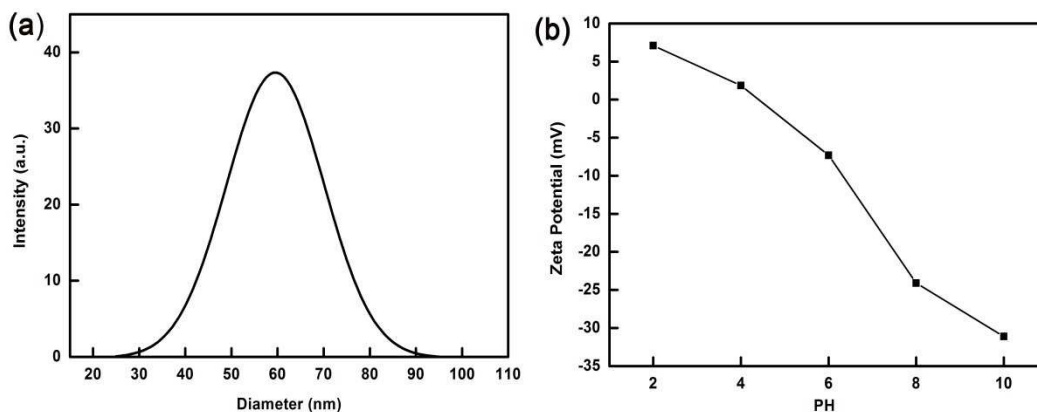

Figure S3 (a) DLS analysis of Ni-NC@PVP. (b) Zeta potential as a function of pH for Ni-NC@PVP dispersed in water.
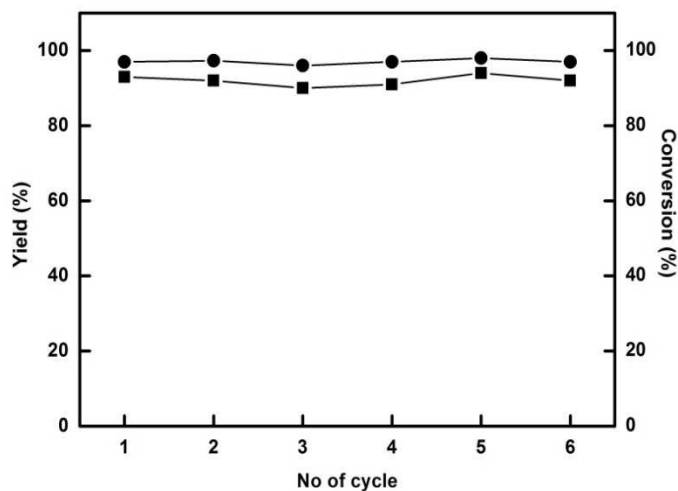

Figure S4 Effect of reaction conditions on the conversion of acetophenone (up) and yield of 1-phenylethanol (below) over Ni-NC@PVP catalyst over six cycles. The yield of 1-phenylethanol and conversion of acetophenone were determined by GC analysis using external standard method.
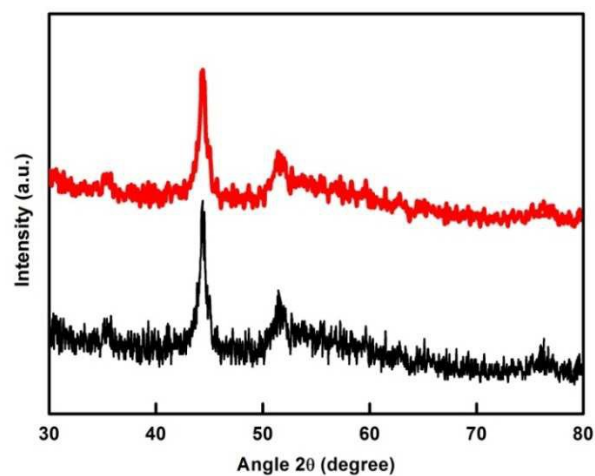
Figure S5 XRD pattern of Ni-NC@PVP before (below) and after (up) the catalytic test reaction.
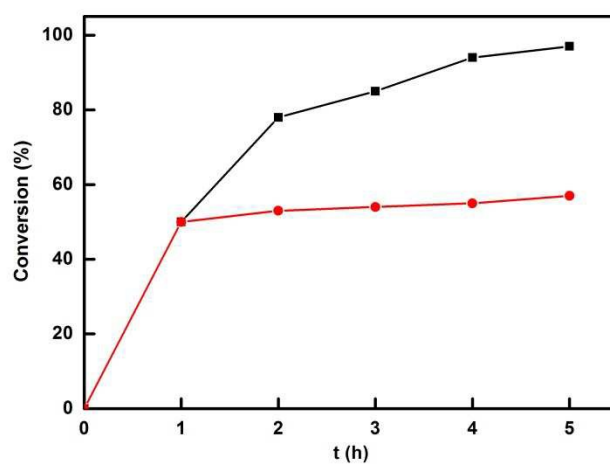

Figure S6 Kinetic profile for the (a) Ni-NC@PVP-catalyzed hydrogenation of acetophenone (square); (b) the reaction mixture at 51 % conversion (cycle) was centrifuged to remove the catalyst.

Table of contents